

# Characteristics of Internal Tides Modulated inside a Mesoscale Warm Eddy based on Single Virtual-moored Slocum Glider observations

JongJin Park<sup>1,2\*</sup>, Gyuchang Lim<sup>2</sup>

<sup>1</sup>School of Earth System Sciences, Kyungpook National University, Daegu, Korea

<sup>2</sup>Kyungpook Institute of Oceanography, Kyungpook National University, Daegu, Korea

Corresponding author: JongJin Park ([jjpark@knu.ac.kr](mailto:jjpark@knu.ac.kr))

## Key Points

- Variability of diurnal and semidiurnal internal tides within a mesoscale warm eddy is detected via virtual-moored single-glider observations.
- Diurnal internal tides' vertical structure changes noticeably for vertical displacement and available potential energy when moving away from the eddy center.
- The vertical structure of diurnal internal tides within a mesoscale eddy varies with distance from the eddy center.

## Abstract

Internal waves are ubiquitous ocean features that significantly contribute to diapycnal mixing, and their modulation by mesoscale eddies is crucial to understanding their propagation and dissipation. From an experiment as a pilot program of the Slocum glider for virtual-moored profiling in a mesoscale eddy, a unique conductivity-temperature-depth (CTD) dataset was obtained and used in this study for examining modulated internal waves within the eddy center. Internal tide variability is detected within the eddy, where diurnal internal tides (DITs) overwhelm other frequency internal waves. DITs' vertical structures change dramatically for vertical displacements and available potential energy (APE), depending on horizontal positions near the eddy center. The observed behavior of DITs' low vertical wavenumbers indicates a cascade of energy from low to high modes, likely due to the hierarchy of wave-eddy interactions. Especially, distinct behavior near the eddy's inner and outer centers indicate different interaction strengths on each regime.

## Plain Language Summary

In this work, actively targeted CTD measurements within a mesoscale eddy were conducted using a single Slocum glider. First, the virtual-mooring mode of a glider was successfully controlled within a 720 m root-mean-square (RMS) around the waypoint and yielded a reliable dataset to capture the internal tide variations. Second, based on the gridded version of raw data in a 1 h and 1 m vertical resolution, diurnal and semidiurnal internal tides are observed in the bandpassed time-depth isothermal displacement maps. Third, the vertical structure of vertical isothermal displacements, as well as the vertical distribution of available potential energies, shows a varying pattern depending on horizontal positions near the eddy center. It is more variable in the inner center and less variable in the outer center. Lastly, there appears a weak clue of energy-cascading behavior from low to higher modes for spectral behavior of low vertical

wavenumbers computed during the observation, indicating that the nonlinear interactions among the waves and the eddy have different strengths in the inner and outer centers: strong in the inner center and weak in the outer center.

## 1 Introduction

Internal waves oscillating in the stratified fluid interior are prevalent in the ocean and play various roles in modulating the ocean environment. Internal waves with tidal frequency are called internal tides (ITs), mostly generated via barotropic tide-bathymetry interactions. Recent research has revealed IT characteristics and roles, such as contributing to diapycnal mixing in the deep ocean (Egbert & Ray, 2000; Munk & Wunsch, 1998; Wunsch & Ferrari, 2004) and transporting considerable amounts of energy over hundreds to thousands of kilometers from the generation site (Alford, 2003; Tian et al., 2003).

Most ITs are unpredictable in their long-range propagation because of frequent encounters with currents and eddies ubiquitous in oceans, varying ITs' propagation speed and direction (Alford et al., 2012; Nash et al., 2012; Kerry et al., 2014). Particularly, mesoscale eddies are critical in modulating ITs. These mesoscale eddies are energetic swirling nonlinear circulations with horizontal scales on the order of 100 km and timescales on the order of a month, typically detected by composite satellite observations on spatial variations in sea surface height (SSH) (Chelton et al., 2007).

Observational studies and numerical simulation analyses have been conducted on the influence of mesoscale eddies on ITs. Nash et al. (2012) reported that ITs over the New Jersey shelf were incoherent and largely unpredictable, possibly due to eddies in their path. Kerry et al. (2014) demonstrated that the location of eddies influenced the spatial pattern of IT propagation near the Luzon Strait. Dunpy and Lamb (2014) numerically showed that the energy flux of ITs was produced in beam-like patterns through a barotropic eddy, whereas passing a mode-one IT through a mode-one baroclinic eddy, scattered energy from the incident mode-one to mode-two and higher. Using a mathematical model, Lelong and Riley (1991) demonstrated that wave-wave-vortex triad interactions could be found between two equal-frequency waves and one vortex and that the vortex acted as a catalyst to facilitate energy transfer between two wave modes.

Along with those theoretical and analytical studies, there were observations based on moorings and ship-based data to prove IT modulations by eddies (Huang et al., 2017 & 2018). Mooring platforms provide suitable temporal resolutions but have limited spatial information in sampling internal wave fields, whereas gliders enable additional internal wave characterization with a better spatial resolution and time and cost-efficiency. In glider implementations, several employed approaches exist, such as virtual-mooring (VM), along-shore transects, across-shore transects, and a zig-zag flight across the wavefronts. In this work, to examine internal wave variability within a mesoscale warm eddy, a virtual-mooring approach is implemented.

Therefore, a single Slocum glider actively moved to a target eddy (Figure 1b) located at 21.03°N and 131.25°E, and repeatedly profiles to an 800 m depth on an average of 0.3 m/s (Figure 1d). This study region is approximately 1000 km apart, eastward from Luzon Strait, an energetic IT generation site. From recent observations (Rainville et al., 2013), significant energy fluxes propagated from the Luzon Strait into the western Pacific for diurnal ITs (DITs) and semidiurnal ITs (SITs), compatible with the results of numerical models (Niwa & Hibiya, 2001). Furthermore, the  $K_1$  and  $O_1$  ITs propagated over a long distance of approximately 2500 km

(Zhao, 2014). From these results, ITs generated at the Luzon Strait propagate into our study region and are modulated due to background current and eddy interactions on their propagation path. In this study, the characteristics of vertical displacements associated with modulated ITs within a mesoscale eddy are examined based on in-situ conductivity-temperature-depth (CTD) measurements using a Slocum glider with a suitable station-keeping performance (Figure 1c).

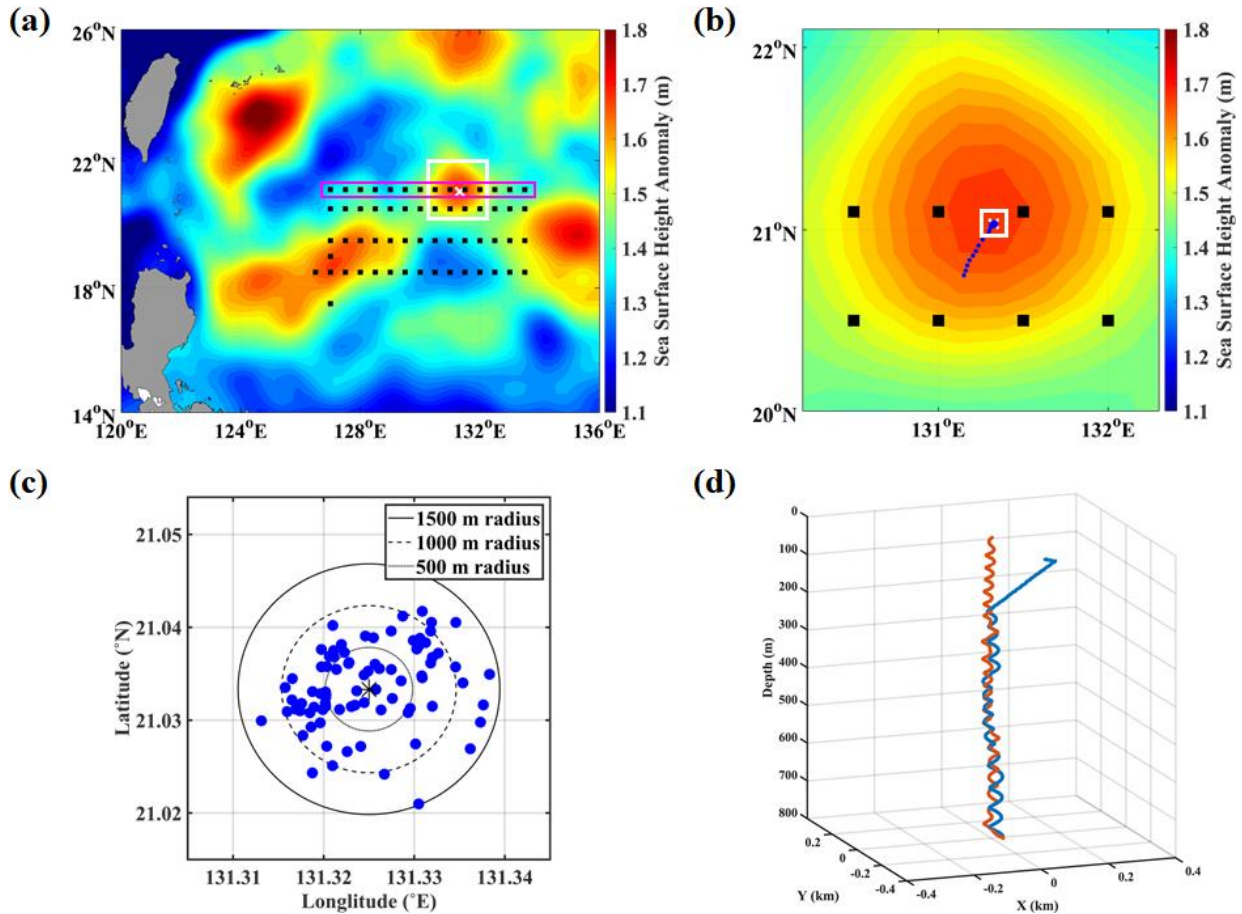


**Figure 1.** (a) Map of sea surface height (SSH) over the northwestern Pacific, including target spot (white cross in the white box), surrounded by warm and cold eddies of variable scale. The black dots indicate the path of R/V *ISABU* along which the conductivity-temperature-depth (CTD) profiles are obtained. Note that the eddy is approximately 1000 km from the energetic region of the Luzon Strait. (b) The white box of (a) is enlarged, where the SSH was obtained on September 11. A glider has moved to the eddy center along the path indicated by the blue dots. (c) The white box of (b) is enlarged. A glider was well controlled to surface within 720 m RMS around the waypoint, resulting in a dependable virtual-mooring mode. (d) The underwater trajectory during a single dive of the Slocum glider attempting to hold the station at the target spot; dive (blue line) and climb (red line). Spiraling motion with a small radius is well maintained, except for the subsurface dive due to drift by the surface current.

## 2 Observations and Methods

### 2.1 Measurements

A Slocum glider is an autonomous underwater vehicle, actively moving to targeted locations and occupying controlled spatial and temporal grids. The glider moves horizontally and vertically by altering buoyancy and carries a suite of sensors measuring CTD, dissolved oxygen, and chlorophyll-a fluorescence. In this study, a single Slocum glider repeatedly profiled from the surface to an 800 m depth in a virtual-mooring mode took on average 2.8 h to complete one cycle and yielded profiles with high vertical and irregular time resolutions from 1.4 h in midpoint to 2.8 h at the top and bottom (Figure 1d). During the cycle, the glider dives and climbs, making a spiral motion with a small radius (Figure 1d), where the trajectory was estimated from the glider's vertical velocity and heading information. When climbing, the glider is drifted due to ambient horizontal currents. Up-casts are better at the holding position than down-casts (Figure 1d), but there is no difference between them regarding the gridded version of raw data (Figures 4-c, d, and S1). The Slocum's rudder-based steering, with a radius smaller than 20 m when rotated by  $180^\circ$ , enhanced the station-keeping performance, resulting in the 720 m RMS of the glider's surfacing spots from the waypoint (Figure 1c) and making no impact on vertical water properties with scales larger than several meters.

The glider was deployed from the research vessel *ISABU* at  $20.71^\circ\text{N}$  and  $131.11^\circ\text{E}$  on September 8, 2018, and actively traveled from the surface to as deep as 800 m in a sawtooth pattern, 42 km northeast from the deployment site to our target while recording the CTD measurements (blue dots in Figure 1b). The target is a mesoscale warm eddy center, identified using level 4 SSH satellite data from the Copernicus Marine Environmental Monitoring Service (CMEMS: <https://marine.copernicus.eu/access-data>). At the eddy center (the white box in Figure 1b), from September 10 to 19, 2018, the glider was operated in a virtual-mooring mode, collecting CTD profiles with a sampling frequency of 4 Hz, resulting in a vertical resolution of on average 0.5 m. During observations, the eddy slowly traveled northward (Figure 2), allowing the glider to naturally scan the eddy center horizontally and vertically.

Raw data have irregular vertical/temporal sampling intervals due to variations in upward/downward speeds of a moving glider due to background currents. Thus, they are gridded to 1 m vertical and 1 h temporal resolutions by linear interpolation. Then, a boxcar filter of 10 m smooths the gridded space-time series to capture internal wave variations at diurnal and semidiurnal frequencies.



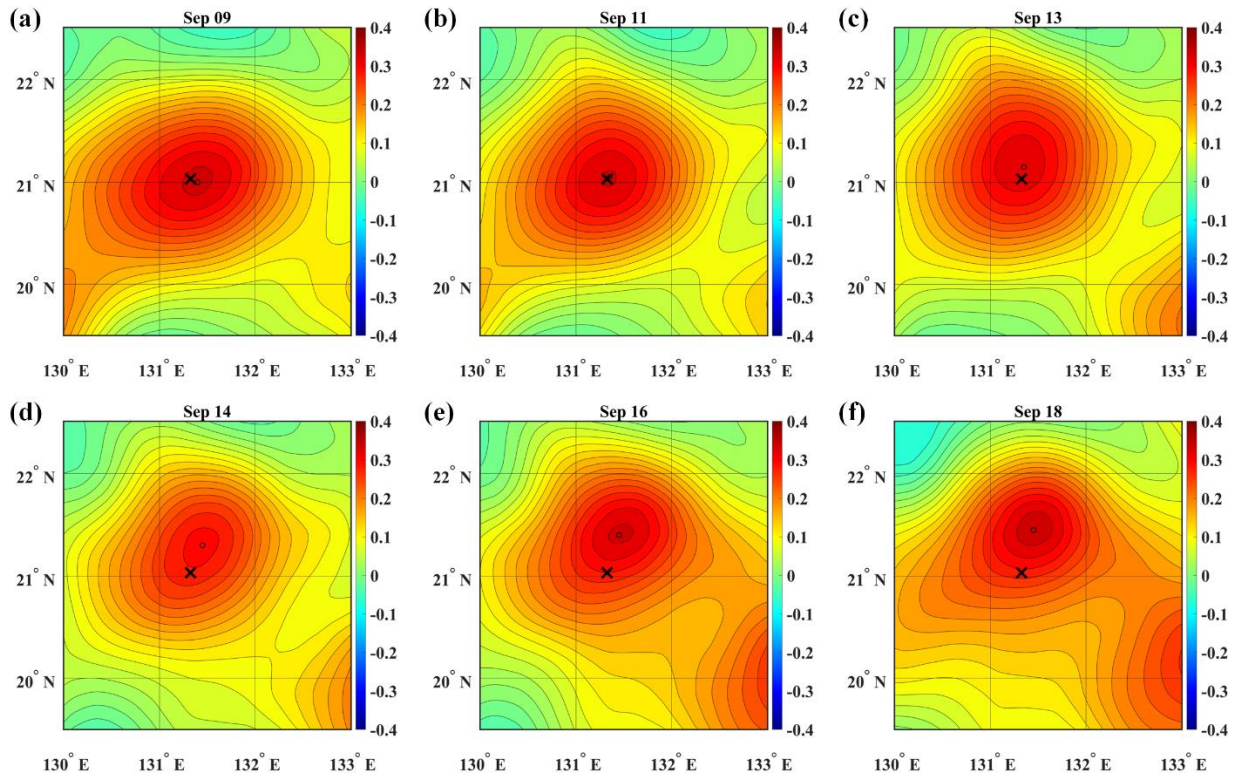


**Figure 2.** Contour map of SSH data (m), showing a moving mesoscale warm eddy during the virtual-moored glider mission; the glider (black dot) scanned the vicinity of the inner-core from Sep. 9 to Sep. 13 (top panels), and the outer-core vicinity from Sep.14 to Sep.18.

From the research vessel (R/V) *ISABU* migrating across the mesoscale warm eddy from September 4 to 7, 2018 (see the purple box in Figure 1a), CTD profiles were collected using the Sea-Bird Electronics (SBE) 911 plus system. Measurements were obtained during up- and down-casts, but here, only the down-cast data were used to depict transects of temperature variability (Figure 3a). All instruments were calibrated before deployment, and data were processed according to manufacturers' specifications.

## 2.2 Mesoscale warm eddy

Due to the lack of observational information for the eddy's 3D structure, the eddy's spatial scales were approximately estimated to be horizontal  $\sim 150$  km and vertical  $\sim 400$  m, based on CTD observations of the R/V *ISABU* (Figure 3a). From the estimations, we divide the observed water column ( $\sim 800$  m) into two layers—the upper (down to 400 m) and lower (from 400 m down to 800 m). Because the eddy migrated northward during the glider mission, glider observation naturally enables high-resolution cross-section scans of the eddy (Figure 2). As a proxy characteristic indicating the eddy's horizontal structure, the relative vorticity was calculated from real-time satellite SSH data via geostrophic balance equations (Figure 3b). Variations of the relative vorticity during the observation period show an abrupt increase between Sep. 14 and 15. Thus, the eddy is horizontally divided into two domains, the inner and outer center, based on the relative vorticity behavior, depending on the distance from the eddy

center. Note that this relative-vorticity-based horizontal structure of the eddy, although being arbitrarily constructed, coincides well with variations of isothermal vertical displacement DIT patterns (Figure 4c).

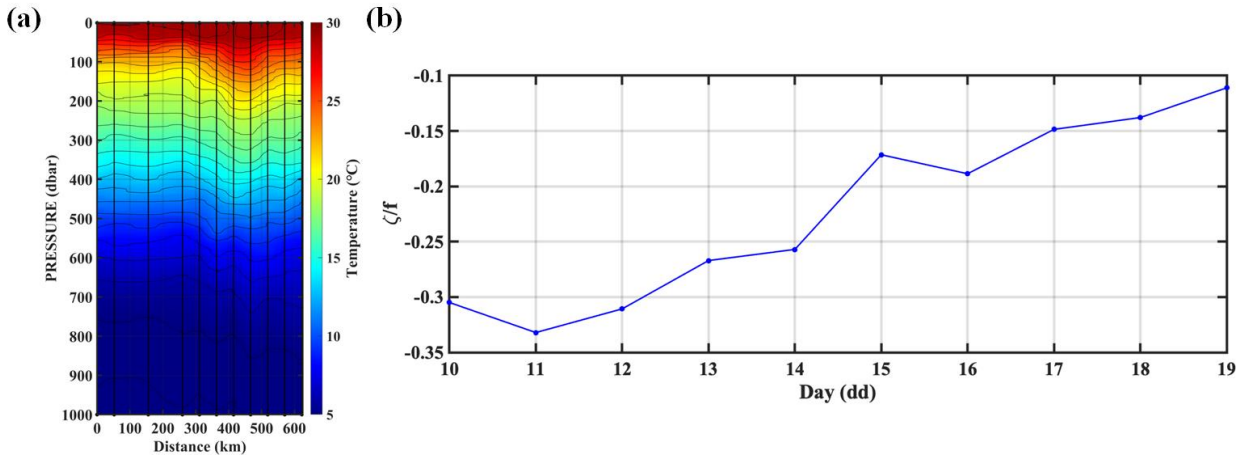


**Figure 3.** (a) The horizontal-vertical map of temperature variations along with isothermal curves obtained from CTD observations of the R/V *ISABU* represents the spatial structure of the eddy, and the bottom of the eddy reaches a depth of 400 m. (b) The vorticity at the glider position was calculated using satellite SSH data; variations of the vorticity regarding the distance from the eddy center is noticeable, especially with an abrupt rise on Sep. 14, indicating a transition.

### 2.3 Vertical displacements

To investigate the behavior of ITs within the eddy, vertical displacements are defined and used for analysis. The vertical displacement is calculated using  $\eta(z, t) = [T(z, t) - \bar{T}(z, t)] / \bar{T}_z(z, t)$  based on the glider CTD measurements. Here,  $T(z, t)$  denotes the gridded temperature measurements, and  $\bar{T}(z, t)$  is the background temperature calculated from averaging  $T(z, t)$  over the entire observation period. The  $\bar{T}_z(z, t)$  is the temperature gradient of  $\bar{T}(z, t)$ ; that is,  $\bar{T}_z(z, t) \equiv \partial \bar{T}(z, t) / \partial z$ .

We first estimated the power spectral density (PSD) of 10°C and 20°C isothermal vertical displacements corresponding to depths of 230 m and 550 m, respectively, using the PWELCH estimation of 50% overlapping segments with a size of 128. DIT is observed to dominantly occupy the vertical displacement variation outside the eddy, although a noticeable SIT contribution occurs inside the eddy (Figure 4b). This behavior means that ITs dominantly contribute to vertical displacements. Thus, displacements associated with DITs and SITs are isolated via a fourth-order phase-preserving Butterworth bandpass filtering, with a central frequency at 1 cpd and a half cpd with a bandwidth of 1/3 cpd.

For examining variations of the vertical IT structure, the wavenumber-frequency spectra were estimated for depth-time vertical displacements—the entire domain and inter/outer domains, respectively. S2 shows the wavenumber-frequency spectra for inner/outer domains. For the comparison with the Garret–Munk spectra model (GM76), we separately projected the wavenumber-frequency spectra onto frequency (S3) and wavenumber domains (S4); here, the frequency spectra are computed over the entire wavenumber bandwidth (S3), whereas the

wavenumber spectra are computed over the selected DIT bandwidth (S4). Note that the power-law slope shows a robust behavior in the wavenumber domain, whereas the frequency domain shows a different behavior of the power-law slope, depending on the horizontal position near the eddy center.

## 2.4 Wentzel–Kramers–Brillouin (WKB) scaling

The glider observation depth reaching 800 m is too shallow compared to the water column's full depth reaching as deep as 5000 m. However, by accounting for the strong stratification near the surface, the depth and amplitude can be effectively scaled (Rainville et al., 2013). Typically, the depth-varying stratification intensifies horizontal velocity, energy density, and energy density flux near the surface where stratification is strong, whereas isothermal displacements are amplified in deep water where stratification is weak. Thus, the depth coordinate is stretched to emphasize the subsurface layer with strong stratification, and the amplitudes are scaled according to WKB normalization (Althaus et al, 2003; Huang et al., 2017) to obtain a description of IT's vertical structure without the complicated influence of variable stratification. The scaled vertical displacement and stretched-depth coordinates are given as

$$\hat{\eta}(z, t) = \eta(z, t) \sqrt{\frac{\bar{N}(z)}{N_0}} \quad (1)$$

and

$$\hat{z} = \int_z^0 \frac{\bar{N}(z')}{N_0} dz', \quad (2)$$

where the caret denotes the WKB-scaled value,  $\bar{N}(z)$  is the time-mean measured buoyancy frequency, and  $N_0 = 7.40 \times 10^{-3}$  is a constant reference buoyancy frequency based on the depth-average buoyancy frequency from our observations. In this stretched coordinate system, the bottom is shallower than in reality. This scaling is equivalent to convert the ocean to one of constant stratification, where the vertical column domain corresponds to ~26% of the stretched water column,  $H_{WKB} = 3100$  m. Therefore, although the glider observations are collected only to the top 800 m, they effectively sample up to a quarter of the density range, enough to cover the eddy structure.

## 2.5 APE

In this study, DIT and SIT energies are computed following the procedure of previous studies (Nash et al., 2005; Zhao et al., 2010). Due to the limitation of glider observations, restricted to CTD profiles, we only consider the depth-integrated APE, calculated using

$$APE(t) = \int_{-H}^0 ape(z, t) dz = \frac{1}{2} \int_{-H}^0 \langle \rho(z, t) N^2(z, t) \eta^2(z, t) \rangle dz, \quad (3)$$

where  $\rho(z, t)$  denotes the water density calculated using TESO 2010 (McDougall & Barker, 2017) from the CTD data,  $H$  denotes the water depth (here, the glider observation depth is used), and the angle bracket denotes an average over one diurnal tidal cycle.  $ape(z, t)$  is the spot APE. The  $N^2(z, t)$  is the squared buoyancy frequency calculated from the potential density smoothed by a 2-day sliding window. For DIT and SIT, the corresponding displacements  $\eta(z, t)$  are isolated via bandpass filtering (Section 2.4).

To examine the characteristics of ITs modulated via interactions among ITs and a mesoscale eddy, we examined the vertical distributional pattern of APEs using the ratio of APE over depth, defined as

$$APEr(t) = \int_{-h}^0 \langle \rho(z, t) N^2(z, t) \eta^2(z, t) \rangle dz / \int_{-H}^0 \langle \rho(z, t) N^2(z, t) \eta^2(z, t) \rangle dz, \quad (4)$$

where  $h$  denotes the bottom depth of a warm eddy, approximately equal to 400 m. The ratio  $APEr$  describes how APEs in the upper layer vary depending on the horizontal position near the eddy center (Figure 5). This can be a clue to the intensity of interactions between ITs and mesoscale eddies.

### 3 Observational Results

#### 3.1 Vertical displacements

In the spectral analysis of two isotherms (20°C and 10°C), with WKB-scaled depths of 330 m and 625 m (Figure 4b), a great peak is observed at the DIT frequency for both. Especially, a noticeable peak at the SIT frequency for 20°C could be due to the second harmonics generation, a result of various wave-wave interactions excited (Dunphy & Lamb, 2014). According to the glider-based observation study (Rainville et al., 2013), similar DIT and SIT energy fluxes are observed to propagate into the WP near the LS. However, from Figure 4 b–d, DIT rather than SIT dominantly contributes to the vertical displacements associated with internal waves. This noticeable weakness in SIT compared to DIT in our study region is consistent with satellite altimeter observations (Zhao, 2014), although there is yet no plausible reason to support this observation. When restricted to the isotherm for 20°C, SIT is comparable to DIT regarding PSD (Figure 4b). This behavior could be due to harmonics generations via wave-wave-vortex triad resonance (Dunphy & Lamb, 2014).

Amplitudes of DIT vertical displacement are weaker in the upper layer of less than 400 m than in the lower layer deeper than 400 m (Figure 4c), whereas SIT shows more complicated variability (Figure 4d). This behavior could be due to nonuniform stratification (stronger (weaker) stratification in the upper (lower) layer), and partly due to wave-vortex interactions within the eddy. Also, the strong to weak variation of vertical displacements is observed in the lower layer over the entire duration, indicating a fortnight cycle in DIT (Figure 4c).



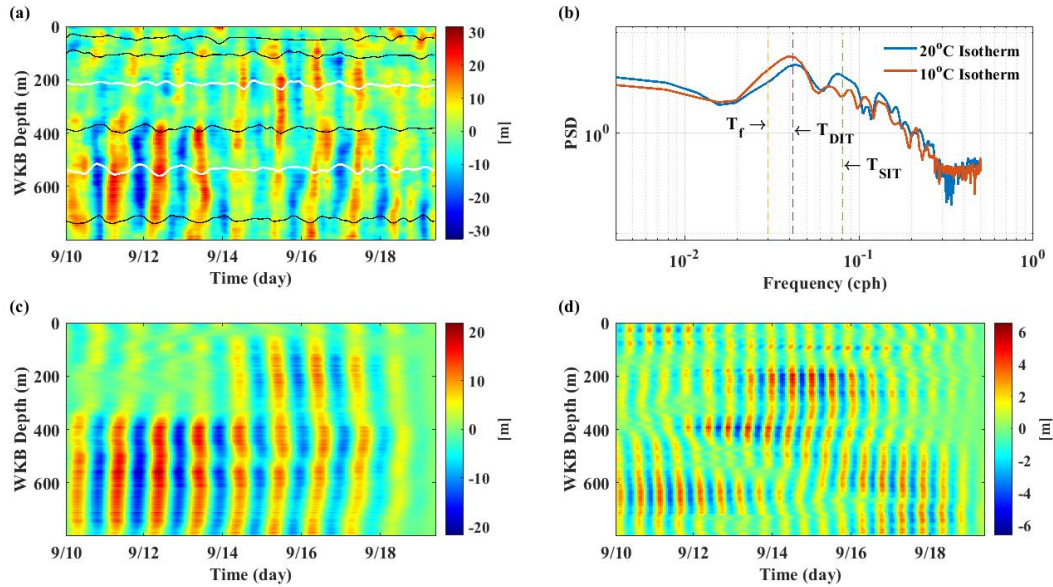


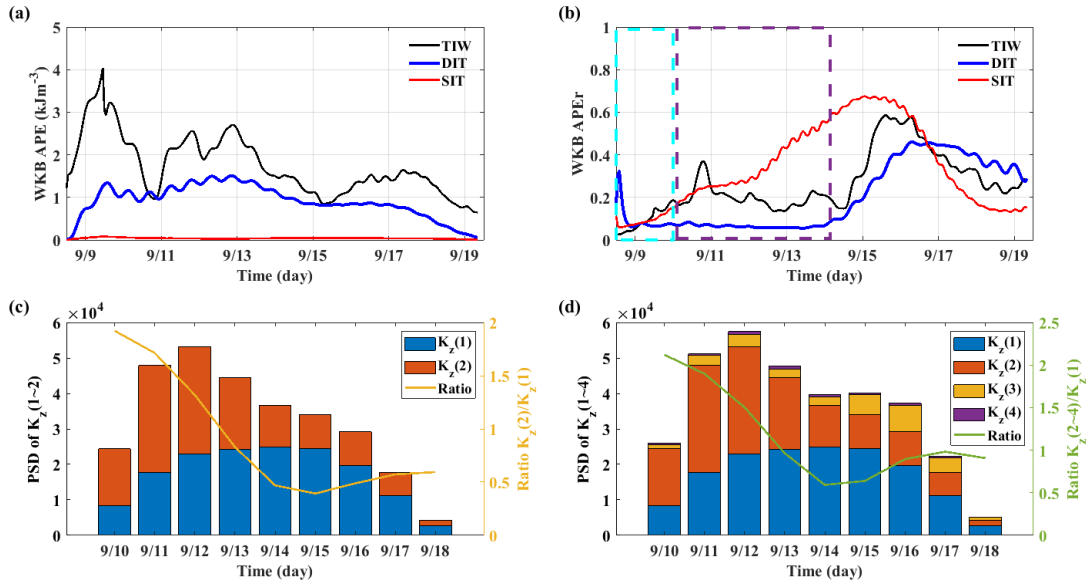
**Figure 4.** (a) The depth-time map of WKB-scaled isothermal displacements is depicted with isotherms corresponding to 29°C, 25°C, 20°C, 15°C, 10°C, and 6°C, where two white lines indicate 20°C and 10°C. (b) The power-spectrum of vertical displacements of two isotherms correspond to 20°C and 10°C, respectively. DIT dominates in the lower layer, whereas SIT is more pronounced in the upper layer rather than in the lower layer, probably due to a second harmonics generation within a mesoscale eddy. (c) Diurnally bandpassed isothermal displacements are depicted, showing a phase discrepancy between the upper and lower layers at the eddy center and gradually becoming in-phase away from the center. (d) Semi-diurnally bandpassed vertical displacements show a complex pattern in magnitudes and phases.

### 3.2 Characteristics of APE

Energy transfer between the vertical modes of internal waves via their interaction with mean fields and mesoscale eddies, such as resonant triad interactions (McComas & Bretherton, 1977), is a critical issue as an energy-cascading mechanism that converts huge barotropic tidal energy into baroclinic ITs and finally dissipates the large-scale energy into smaller scales, leading to various vertical mixings.

We first computed the integrated APE for bandpassed ITs, say DIT and SIT, by following procedures described in Section 2.6, and Figure 5 shows their variations with time. First, the smooth up-down variations of APE for DIT (Figure 5a) could be due to a fortnight rhythm. Second, to examine the vertical APE distribution near the eddy center, we used the  $APE_r$  defined in Eq. (4) by setting  $h = 400$  m, assuming that the eddy has a strong impact on ITs in the layer above  $h = 400$  m. DIT shows a dramatic change over inner and outer centers (Figure 5b), indicating that APEs (magnitude of vertical displacements) are focused on the lower layer (weak vortical fields) during staying in the inner center. However, SIT shows a different behavior by being relatively uniformly distributed over the water column during moving from the inner to outer centers (Figure 5b). This focusing DIT behavior indicates an unclear mechanism underlying the interactions between internal waves in our restricted dataset.

282



283

**Figure 5.** The top panel shows available depth-integrated APEs. (a) APEs of total internal waves (TIW), DIT, and SIT are shown for the entire glider observation period. (b) APE ratios ( $APEr$ ) of the upper layer (eddy) to the entire water column are plotted during the same period. A cyan broken-line box denotes the pre-VM interval during which the glider moves in a zig-zag manner to a target station, and the purple box denotes the eddy center (target) under VM measurements. In the bottom panel, 24-h averaged PSDs of vertical DIT wavenumbers are shown. (c) PSDs of the two lowest vertical wavenumbers are plotted over the virtual mooring duration, along with the ratio (right y-axis). (d) PSDs of the four lowest vertical wavenumbers are plotted, along with the ratio.

A direct investigation of energy cascades among vertical modes is possible in numerical simulation analysis (Dunphy & Lamb, 2014), where a sole coherent SIT is incident on the eddy of a well-known structure. However, it is challenging to be conducted based on in-situ measurements because of the lack of information on the eddy's 3D structure and wide bandwidths of incoming internal waves. Especially, it becomes harder using limited datasets, such as glider observations. Thus, we take an alternative approach to examine the frequency spectra structures for low vertical wavenumber bandwidths using the vertical wavenumber spectral estimations, calculated for diurnally bandpassed 1-h gridded vertical displacements (DIT) during the entire observation. Then, by averaging those PSDs over 24 h in a nonoverlapping manner, we obtained diurnal wavenumber spectral estimates. Here, the four lowest vertical wavenumbers are chosen and examined for energy-cascading behavior, depending on positions near the eddy center. From Figures 5 c and d, the summed variance at the four lowest vertical wavenumbers of DIT varies from large to small, similar to a fortnight IT rhythm. For the distribution of variance over the four lowest wavenumbers, the contribution of the first-lowest wavenumber increases as it moves from the inner to outer centers. This characteristic behavior is a qualitative clue of energy-cascading variations (strong in the inner center and weak in the outer center). A similar analysis was performed on overlapping time-

depth data segments for wavenumber-frequency spectral densities and showed similar behavior, although having different ratios (S5). Also, S6 shows the significance of PSD intervals based on wavenumber-frequency spectra, indicating a cascading tendency in the low vertical wavenumbers over the wide frequency bandwidths.

For energy-cascading processes in the wavenumber-frequency domains, several mechanisms were theoretically investigated and well established (Polzin & Lvov, 2011). Especially, the cascading process in vertical wavenumbers between two internal equal-frequency waves is well explained for wave-wave-vortex triad interaction (Lelong & Riley, 1991). According to the work of Dunphy & Lamb (2014), the incoming SIT shows a cascading process from low to high modes in vertical dynamic modes and frequencies (harmonics). However, for a multitude of incoming internal waves with different vertical modes and frequencies within a mesoscale eddy, numerical studies have not been conducted. Thus, our observational results are worthwhile for in-depth future observational studies.

#### 4 Discussion and Conclusions

In this study, we actively navigated a single Slocum glider to a targeted center of a mesoscale eddy and performed virtual-moored observations at a single point during the eddy's migrating motion. Because the glider is profiling in a high-frequency spiraling motion with a small radius, less impact on IT observations occurs due to background currents. Also, by applying the wide bandpass widths to the gridded dataset with a temporal resolution of 1 h and vertical resolution of 1 m, the doppler effect induced by the glider's motion is well reduced. Our observations show stronger DIT fields than other internal wavefields, including SITs. This characteristic could be due to different poleward DIT and SIT refractions radiated from the Luzon Strait, as numerically verified in the work of Zhao (2014). However, comparable energy DIT and SIT fluxes propagate into the western Pacific near the generation site, the Luzon Strait (Rainville et al., 2013). The finding that the SIT's power spectra of the 20°C isotherm are larger than the 10°C (Figure 4b) indicates second harmonics generation of higher-mode DIT via eddy-wave interaction, reported in the work of Dunphy & Lamb (2014).

The focusing behavior of DIT's APEs observed in the inner center is a clue to strong modulation on DIT by the eddy via nonlinear interactions between DIT wavefields and the vortex. To unveil the underlying dynamics, additional observations with longer duration and velocity measurements are required.

For energy-cascading processes, variations of cascading strength depending on positions near the eddy center are tentatively described in terms of the four lowest vertical wavenumbers for the DIT wavefield. Compared to the work of Dunphy & Lamb (2014, see Figure 13 therein), the contributions of the four lowest wavenumbers to DIT variance are not clearly distinguished among the lowest wavenumbers. However, note that different behavior is observed in the eddy's inner and outer centers (Figures 5 c and d). This finding can be a qualitative clue to resonant triad interactions among wave-wave-vortex varying on positions near the eddy center (strong in the inner center and weak in the outer center). The relationship between the strength of interactions and horizontal positions within the eddy should be established on further observations. There is also a probable relationship between characteristics dependent on horizontal positions within the eddy and relative vorticity (Figure 3). Its relation must also be reinforced by additional observations.

## Acknowledgments

The authors acknowledge the help of BongJoon Kim, YunChang Kwak, and the KAOS team for Glider operation. We also sincerely acknowledge Dr. Sok-Kuh Kang and crews of R/V ISABU for their warm cooperation during hydrographic measurements for cruises.

The altimeter products were produced by Ssalto/Duacs and distributed by Aviso+, with support from Cnes (<https://www.aviso.altimetry.fr>). This research was a part of the project titled 'Development of the core technology and establishment of the operation center for underwater gliders', funded by the Ministry of Oceans and Fisheries, Korea. This research was also supported by the research programs of the Korea Institute of Ocean Science and Technology (PE99654).

## References

- Alford, M. H. (2003). Redistribution of energy available for ocean mixing by long-range propagation of internal waves. *Nature*, 423, 159–162. <https://doi.org/10.1038/nature01628>
- Alford, M. H., Mickett, J. B., Zhang, S., MacCready, P., Zhao, Z., & Newton, J. (2012). Internal waves on the Washington continental shelf. *Oceanography*, 25, 66–79. <https://doi.org/10.5670/oceanog.2012.43>
- Althaus, A. M., Kunze, E., & Sanford, T. B. (2003). Internal tide radiation from Mendocino Escarpment. *Journal of Physical Oceanography*, 41, 2211–2222. [https://doi.org/10.1175/1520-0485\(2003\)033<1510:ITRFME>2.0.CO;2](https://doi.org/10.1175/1520-0485(2003)033<1510:ITRFME>2.0.CO;2)
- Chelton, D. B., Schlax, M. G., Samelson, R. M., & de Szoeke, R. A. (2007). Global observations of large oceanic eddies. *Geophysical Research Letters*, 34, L15606. <https://doi.org/10.1029/2007GL030812>
- Dunphy, M., & Lamb, K. G. (2014). Focusing and vertical mode scattering of the first mode internal tide by mesoscale eddy interaction. *Journal of Geophysical Research: Oceans*, 119, 523–536. [doi:10.1002/2013JC009293](https://doi.org/10.1002/2013JC009293)
- Egbert, G. D., & Ray, R. D. (2000). Significant dissipation of tidal energy in the deep ocean inferred from satellite altimeter data. *Nature*, 405, 775–778. [doi:10.1038/35015531](https://doi.org/10.1038/35015531)
- Huang, X., Wang, Z., Zhang, Z., Yang, Y., Zhou, C., Yang, Q., Zhao, W., & Tian, J. (2018). Role of mesoscale eddies in modulating the semidiurnal internal tide: Observation results in the northern South China Sea. *Journal of Physical Oceanography*, 48, 1749–1770. [doi:10.1175/JPO-D-17-0209.1](https://doi.org/10.1175/JPO-D-17-0209.1)
- Huang, X., Zhang, Z., Zhang, X., Qian, H., Zhao, W., & Tian, J. (2017). Impacts of a mesoscale eddy pair on internal solitary waves in the northern South China Sea revealed by Mooring Array Observations. *Journal of Physical Oceanography*, 47, 1539–1554. [doi:10.1175/JPO-D-16-0111.1](https://doi.org/10.1175/JPO-D-16-0111.1)
- Gill, A. E. (1982). *Atmosphere-ocean dynamics*. Academic Press.
- Kerry, C. G., Powell, B. S., & Carter, G. S. (2014). The impact of subtidal circulation on internal tide generation and propagation in the Philippine Sea. *Journal of Physical Oceanography*, 44, 1386–1405. [doi:10.1175/JPO-D-13-0142.1](https://doi.org/10.1175/JPO-D-13-0142.1)

- Lelong, M. -P., & Riley, J. J. (1991). Internal wave-vortical mode interactions in strongly stratified flows. *Journal of Fluid Mechanics*, 232, 1–19. [doi:10.1017/S0022112091003609](https://doi.org/10.1017/S0022112091003609)
- McComas, C. H., & Bretherton, F. P. (1977). Resonant interaction of oceanic internal waves. *Journal of Geophysical Research*, 82, 1397–1412. [doi:10.1029/JC082i009p01397](https://doi.org/10.1029/JC082i009p01397)
- McDougall, T. J., & Barker, P. M. (2017). Getting started with TEOS-10 and the Gibbs Seawater (GSW) Oceanographic Toolbox.
- Munk, W., & Wunsch, C. (1998). Abyssal recipes II: Energetics of tidal and wind mixing. *Deep Sea Research Part I*, 45, 1977–2010. [doi:10.1016/S0967-0637\(98\)00070-3](https://doi.org/10.1016/S0967-0637(98)00070-3)
- Nash, J. D., Alford, M. H., & Kunze, E. (2005). Estimating internal wave energy fluxes in the ocean. *Journal of Atmospheric and Oceanic Technology*, 22, 1551–1570. [doi:10.1175/JTECH1784.1](https://doi.org/10.1175/JTECH1784.1)
- Nash, J. D., Kelly, S. M., Shroyer, E. L., Moum, J. N., & Duda, T. F. (2012). The unpredictable nature of internal tides on continental shelves. *Journal of Physical Oceanography*, 42, 1981–2000. [doi:10.1175/JPO-D-12-028.1](https://doi.org/10.1175/JPO-D-12-028.1)
- Niwa, Y., & Hibiya, T. (2001). Numerical study of the spatial distribution of the M2 internal tide in the Pacific Ocean. *Journal of Geophysical Research: Oceans*, 106, 22441–22449. [doi:10.1029/2000JC000770](https://doi.org/10.1029/2000JC000770)
- Pedlosky, J. (2003). Waves in the ocean and atmosphere: Introduction to wave dynamics. Springer.
- Polzin, K. L., & Lvov, Y. V. (2011). Toward regional characterizations of the oceanic internal wavefield. *Reviews of Geophysics*, 49, RG4003. [doi:10.1029/2010RG000329](https://doi.org/10.1029/2010RG000329)
- Rainville, L., Lee, C. M., Rudnick, D. L., & Yang, K.-C. (2013). Propagation of internal tides generated near Luzon Strait: Observations from autonomous gliders. *Journal of Geophysical Research: Oceans*, 118, 4125–4138. [doi:10.1002/jgrc.20293](https://doi.org/10.1002/jgrc.20293)
- Tian, J., Zhou, L., Zhang, X., Liang, X., Zheng, Q., & Zhao, W. (2003). Estimates of M2 internal tide energy fluxes along the margin of northwestern Pacific using TOPEX/POSEIDON altimeter data. *Geophysical Research Letters*, 30, 1889. <https://doi.org/10.1029/2003GL018008>
- Wunsch, C., & Ferrari, R. (2004). Vertical mixing, energy, and the general circulation of the oceans. *Annual Review of Fluid Mechanics*, 36, 281–314. <https://doi.org/10.1146/annurev.fluid.36.050802.122121>
- Zhao, Z. (2014). Internal tide radiation from the Luzon Strait. *Journal of Geophysical Research: Oceans*, 119, 5434–5448. [doi:10.1002/2014JC010014](https://doi.org/10.1002/2014JC010014)
- Zhao, Z., Alford, M. H., MacKinnon, J. A., & Pinkel, R. (2010). Long-range propagation of the semidiurnal internal tide from the Hawaiian Ridge. *Journal of Physical Oceanography*, 40, 713–736. [doi:10.1175/2009JPO4207.1](https://doi.org/10.1175/2009JPO4207.1)